Mixed-Valent Mn_{16}-Containing Heteropolyanions: Tuning of Oxidation State and Associated Physicochemical Properties

Ali Haider,[†,□] Masooma Ibrahim,[†,☆,□] Bassem S. Bassil,[†,‡] Akina M. Carey,[†] Anh Nguyen Viet,[†] Xiaolin Xing,[†] Wassim W. Ayass,[†] Juan F. Miñambres,[†] Rongji Liu,[§] Guangjin Zhang,[§] Bineta Keita,[∥,△] Valeriu Mereacre,[⊥] Annie K. Powell,[⊥,#] Kamil Balinski,[▽] Alpha T. N'Diaye,[○] Karsten Küpper,[▽] Han-Yi Chen,[◆,¶] Ulrich Stimming,[◆,¶,◇] and Ulrich Kortz[*,†]

[†]Department of Life Sciences and Chemistry, Jacobs University, P.O. Box 750 561, 28725 Bremen, Germany

[‡]Department of Chemistry, Faculty of Sciences, University of Balamand, P.O. Box 100, Tripoli, Lebanon

[§]Key Laboratory of Green Process and Engineering, Institute of Process Engineering, Chinese Academy of Sciences, 100190, Beijing, China

[∥]Université Paris-Sud, Laboratoire de Chimie-Physique, UMR 8000 CNRS, Orsay, F-91405, France

[⊥]Institute of Nanotechnology, Karlsruhe Institute of Technology (KIT), Hermann-von-Helmholtz Platz 1, 76344 Eggenstein-Leopoldshafen, Germany

[#]Institute of Inorganic Chemistry, Karlsruhe Institute of Technology (KIT), Engesserstrasse 15, 76131 Karlsruhe, Germany

[▽]Department of Physics and Center of Physics and Chemistry of New Materials, Osnabrück University, D-49069 Osnabrück, Germany

[○]Lawrence Berkeley National Laboratory, Berkeley, California 94720, United States

[◆]TUM CREATE, 1 CREATE Way, #10-02 CREATE Tower, 138602 Singapore

[¶]Department of Chemistry, Technische Universität München, Lichtenbergstraße 4, 85748 Garching, Germany

[◇]School of Chemistry, Bedson Building, Newcastle University, Newcastle upon Tyne, NE1 7RU, United Kingdom

ABSTRACT: The two 16-manganese-containing, Keggin-based 36-tungsto-4-silicates $[Mn^{III}_{10}Mn^{II}_{6}O_6(OH)_6(PO_4)_4(A\text{-}\alpha\text{-}SiW_9O_{34})_4]^{28-}$ (**1**) and $[Mn^{III}_{4}Mn^{II}_{12}(OH)_{12}(PO_4)_4(A\text{-}\alpha\text{-}SiW_9O_{34})_4]^{28-}$ (**2**) have been prepared by reaction of the trilacunary Keggin precursor $[A\text{-}\alpha\text{-}SiW_9O_{34}]^{10-}$ with either $Mn(OOCCH_3)_3{\cdot}2H_2O$ (for **1**) or $MnCl_2{\cdot}4H_2O$ (for **2**), in aqueous phosphate solution at pH 9. Polyanions **1** and **2** comprise mixed-valent, cationic $\{Mn^{III}_{10}Mn^{II}_{6}O_6(OH)_6\}^{24+}$ and $\{Mn^{III}_{4}Mn^{II}_{12}(OH)_{12}\}^{24+}$ cores, respectively, encapsulated by four phosphate groups and four $\{SiW_9\}$ units in a tetrahedral fashion. Both polyanions were structurally and compositionally characterized by single-crystal XRD, IR, thermogravimetric analysis, and X-ray absorption spectroscopy. Furthermore, studies were performed probing the magnetic, electrochemical, oxidation catalytic, and Li-ion battery performance of **1** and **2**.

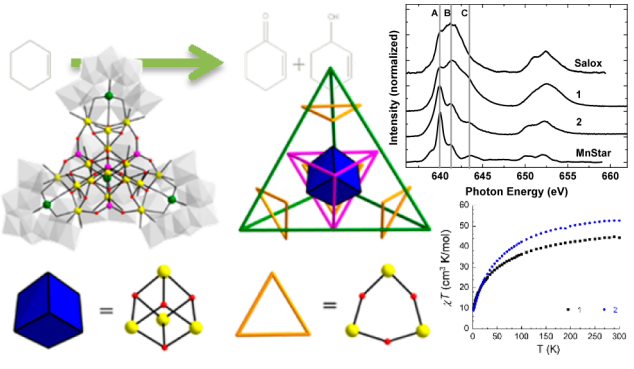

INTRODUCTION

Condensation reactions of simple oxoanions of early transition metals in high oxidation states (e.g., V^V, Mo^{VI}, W^{VI}) in acidic, aqueous medium give rise to the formation of polynuclear structures known as polyoxometalates (POMs).[1] In this process, many factors, such as pH, temperature, concentration and ratio of reagents, as well as counter cations are crucial. Such phenomenon leads to a large number of novel POM structures with a vast variety in terms of shape, size, and composition, leading to interesting combinations of physiochemical properties with potential applications in areas ranging from heterogeneous and homogeneous catalysis to biomedical sciences.[2] Recently, POMs have been reported as promising electrode materials for energy storage applications such as lithium-ion batteries (LIBs), sodium-ion batteries, and supercapacitors.[3] Removal of one or more MO_6 octahedra from plenary structures such as the Keggin ion (e.g., $[PW_{12}O_{40}]^{3-}$) or the Wells–Dawson ion (e.g., $[P_2W_{18}O_{62}]^{6-}$) results in so-called lacunary (vacant) derivatives (e.g., monolacunary $[PW_{11}O_{39}]^{7-}$, trilacunary $[P_2W_{15}O_{56}]^{12-}$), which can be considered as inorganic multidentate ligands, allowing for stabilization of most *d*- and *f*-block metal ions.[1,2]

First row transition metal-containing heteropolytungstates are probably the largest subclass of POMs due to their structural, electronic, redox, magnetic, optical, and catalytic properties, resulting in numerous studies on such compounds in many different areas of science.[2c,4] POMs can be synthesized using conventional, "open-beaker" conditions or by hydrothermal methods, with the latter frequently leading to extended POM-based solid-state networks, rather than discrete molecular polyanions.[4]

In particular, the class of manganese-containing heteropolytungstates is well-established and comprises many members. The number of incorporated manganese centers within these POMs ranges from 1 to 40, including some mixed-valent species (mostly common oxidation states II, III, or IV). Some prominent examples include $\{Mn^{II}P_2W_{17}\}$,[5a] $\{Mn^{II}/Mn^{III}/Mn^{IV}AlW_{11}\}$,[5b] $\{Mn^{II}(SiW_{10})_2\}$,[5c] $\{Mn^{II}(PW_7)_2\}$,[5d] $\{Mn^{III}(SiW_9)_2\}$,[5e] $\{Mn^{III}{}_2SiW_{10}\}$,[6a] $\{Mn^{II}{}_2As_2W_{19}\}$,[6b] $\{Mn^{II}{}_2W_5(P_2W_{12})_3\}$,[6c] $\{Mn^{II}{}_2(PW_9)_2\}$,[6d] $\{Mn^{II}Mn^{III}SiW_{10}\}$,[6e] $\{Mn^{III}{}_2W_{17}\}$,[6f] $\{Mn^{II}{}_2(SiW_8)_2\}$,[6g] $\{Mn^{II}{}_3SiW_9\}$,[7a,g] $\{Mn^{II}{}_3(SiW_{11})_3\}$,[7b] $\{Mn^{II}{}_3(AsW_9)_2\}$,[7c] $\{Mn^{II}Mn^{III}{}_2SiW_9\}$,[7d] $\{Mn^{III}{}_3(PW_9)_2\}$,[7e] $\{Mn^{III}{}_3SiW_9\}$,[7f,g] $\{Mn^{II}{}_4(PW_9)_2\}$,[8a] $\{Mn^{II}{}_4(P_2W_{15})_2\}$,[8b] $\{Mn^{II}{}_3Mn^{III}/Mn^{II}Mn^{III}{}_3(PW_9)_2\}$,[8c] $\{Mn^{II}{}_4(As_2W_{15})_2\}$,[8d] $\{Mn^{II}{}_4(XW_9)_2\}$ (X = Si, Ge),[8e,f] $\{Mn^{II}{}_4(SiW_{10})_2\}$,[8g] $\{Mn^{III}{}_3Mn^{IV}P_2W_{15}\}$,[8h] $\{Mn^{II}{}_4P_8W_{48}\}$,[8i] $\{Mn^{II}{}_2Mn^{III}{}_2(P_2W_{15})_2\}$,[8j] $\{Mn^{III}{}_3Mn^{IV}SiW_9\}$,[7g,8k] $\{Mn^{III}{}_5(SiW_9)_2\}$,[9] $\{Mn^{II}{}_6(PW_9)_2(PW_6)\}$,[10a] $\{Mn^{II}{}_2Mn^{III}{}_4(XW_9)_2\}$ (X = Si, Ge),[10b] $\{Mn^{II}{}_6(GeW_{10})_3\}$,[10c] $\{Mn^{II}{}_6GeW_6(GeW_9)_2\}$,[10d] $\{Mn^{II}{}_4Mn^{III}{}_2(SiW_8)(SiW_9)(SiW_{10})\}$,[10e] $\{Mn^{II}{}_3Mn^{III}{}_3(SiW_{10})_3\}$,[10f] $\{Mn^{II}{}_7(XW_9)_2(XW_8)_2\}$ (X = Ge, Si),[11a,b] $\{Mn^{III}{}_6Mn^{IV}(P_2W_{15})_2\}$,[11c] $\{Mn^{II}{}_7(Si_2W_8)_2(Si_2W_{10})_2\}$,[11d] $\{Mn^{II}{}_8P_8W_{48}\}$,[12a] $\{Mn^{II}{}_8(GeW_{10})_3\}$,[12b] $\{Mn^{II}{}_{10}(SiW_9)_4\}$,[11d] $\{Mn^{II}{}_4Mn^{III}{}_6(SiW_9)_2(SiW_6)_2\}$,[13] $\{Mn^{II}{}_4Mn^{III}{}_6Mn^{IV}{}_2(SiW_6)_2\}$,[14] $\{Mn^{II}Mn^{III}{}_{13}(PW_9)_4\}$,[15a] $\{Mn^{III}{}_6Mn^{IV}{}_8W_{48}\}$,[15b] $\{Mn^{II}{}_{19}(SiW_{10})_6\}$,[16] and $\{Mn_{40}(P_8W_{48})(P_2W_{14})_4(P_2W_{15})_8\}$.[17] Moreover, other mixed-metal POMs containing manganese together with other 3d or 4f metal ions are also known.[18]

Recently, Kortz and Bonchio have shown that the acetate-capped, mixed-valence tetramanganese-containing 9-tungstosilicate $[Mn^{III}{}_3Mn^{IV}O_3(CH_3COO)_3(A\text{-}\alpha\text{-}SiW_9O_{34})]^{6-}$ displays photocatalytic water oxidation properties.[19] In the same year, Su and co-workers showed that the dimanganese(III)-incorporated δ-Dawson ion $[(WO_5)_3W_{14}Mn^{III}{}_2O_{44}Cl_2]^{12-}$ catalyzes hydrogen evolution.[6f]

Our group has been interested for many years in the synthesis and characterization of discrete-molecular heteropolytungstates containing high-nuclearity 3d-metal assemblies. For example, we have reported the $\{Co_{16}\}$-containing 36-tungsto-4-phosphate, -silicate, and -germanate $[\{Co_4(OH)_3PO_4\}_4(A\text{-}\alpha\text{-}XW_9O_{34})_4]^{32-}$ (X = P, Si, Ge), each composed of four $\{Co_3XW_9\}$ units connected in a tetrahedral fashion to a $\{Co_4O_4\}$ cubane unit via four $\{PO_4\}$ groups.[20] These assemblies proved to possess single-molecule magnet (SMM) behavior. Meanwhile, Wang and co-workers have shown that these compounds can act as water oxidation catalysts.[21] Recently, we reported the iron(III) analogues $[Na_2Fe_{14}(OH)_{12}(PO_4)_4(A\text{-}\alpha\text{-}XW_9O_{34})_4]^{20-}$ (X = Si, Ge), where the inner cubane is heterometallic, being occupied by two iron and two sodium ions.[22] All of these polyanions were synthesized in the presence of phosphate ions and in basic aqueous medium, which is somewhat unusual for the synthesis of transition metal-containing POMs, as mostly acidic conditions are preferable.

As a continuation of our work on $\{M_{16}\}$-containing polyanions, we report herein the synthesis and characterization of two mixed-valence Mn_{16}-containing 36-tungsto-4-silicates.

EXPERIMENTAL SECTION

Materials and Physical Measurements. The precursor salt $Na_{10}[A\text{-}\alpha\text{-}SiW_9O_{34}]\cdot 23H_2O$ was prepared according to the published procedure and characterized by FT-IR spectroscopy.[23] All other reagents were used as purchased without further purification. Infrared spectra were recorded on a Nicolet Avatar 370 FT-IR spectrophotometer using KBr pellets. The following abbreviations were used to assign peak intensities: w = weak, m = medium, and s = strong. Thermogravimetric analysis was carried out on a TA Instruments SDT Q600 thermobalance with a 100 mL/min flow of nitrogen; the temperature was ramped from room temperature to 500 °C at a rate of 5 °C/min. Elemental analysis for **NaCs-1** and **NaRb-2** was performed by CNRS, Service Central d'Analyze, Solaize, France.

Synthesis of $Na_{19.5}Cs_{8.5}[\{Mn^{III}{}_{10}Mn^{II}{}_6O_6(OH)_6(PO_4)_4\}(A\text{-}\alpha\text{-}SiW_9O_{34})_4]\cdot 90H_2O$ ***(NaCs-1).*** To a solution of $Mn(OOCCH_3)_3\cdot 2H_2O$ (0.32 g, 1.19 mmol) in 20 mL of H_2O, 0.50 g (0.17 mmol) was added $Na_{10}[A\text{-}\alpha\text{-}SiW_9O_{34}]\cdot 23H_2O$, and the mixture was stirred until a clear dark solution was obtained. The pH of the mixture was then raised to 9 by adding solid Na_3PO_4, and the mixture was stirred for 2 h at room temperature. The turbid black-brown solution was centrifuged (10 min at 4000 rpm) and then decanted. A few drops of 1 M CsCl solution were added to the clear solution, which was then allowed to evaporate in an open vial at room temperature. After about a week, a brown crystalline product appeared, which was collected by filtration and air-dried. Yield 140 mg (57%). IR (2% KBr pellet, ν/cm ^{1}): 1090(m), 944(w), 943(m) 742(m), 899(m), 798(w), 723(w), 524(w); see Figure S1. Elemental analysis (%) for $Na_{19.5}Cs_{8.5}[\{Mn^{III}{}_{10}Mn^{II}{}_6O_6(OH)_6(PO_4)_4\}(A\text{-}\alpha\text{-}SiW_9O_{34})_4]\cdot 90H_2O$, calculated (found): Na 3.31 (3.57), Cs 8.33 (8.40), P 0.91 (0.96), Mn 6.48 (6.20), W 48.79 (48.30), Si 0.83 (0.86).

Synthesis of $Na_{18}Rb_{10}[Mn^{III}{}_4Mn^{II}{}_{12}(OH)_{12}(PO_4)_4(A\text{-}\alpha\text{-}SiW_9O_{34})_4]\cdot 75H_2O$ ***(NaRb-2).*** $MnCl_2\cdot 4H_2O$ (0.24 g, 1.21 mmol) was dissolved in 20 mL of H_2O, and then $Na_{10}[A\text{-}\alpha\text{-}SiW_9O_{34}]\cdot 23H_2O$ (0.50 g, 0.17 mmol) was added. The pH of the solution was adjusted to 9 by addition of solid Na_3PO_4, and then the resulting dark brown solution was stirred for 1 h at room temperature. After filtration, 3−4 drops of 1.0 M RbCl solution were added to the filtrate, which was allowed to evaporate in an open vial at room temperature. Dark brown crystals started to appear after a week, which were then collected by filtration and air-dried. Yield 120 mg (53%). IR (2% KBr pellet, ν/cm ^{1}): 1096(m), 988(w), 938(w), 891(m), 806(m), 714(w), 518(w); see Figure S1. Elemental analysis (%) for $Na_{18}Rb_{10}[Mn^{II}{}_{12}Mn^{III}{}_4(OH)_{12}(PO_4)_4(A\text{-}\alpha\text{-}SiW_9O_{34})_4]\cdot 75H_2O$ calculated (found): Na 3.20 (3.48), Rb 6.57 (6.84), P 0.95 (1.00), Mn 6.76 (6.44), W 50.95 (50.00), Si 0.86 (0.89).

Synthesis of SBA-15. 8.0 g of P_{123} gel (Sigma-Aldrich) was added to 40 mL of 2 M HCl and 208 mL of H_2O. This mixture was stirred initially for 2 h in a water bath at 35 °C until it was completely dissolved. Then, 18 mL of tetraethylorthosilicate (TEOS) was added dropwise, and the mixture was kept stirring for 4 h. Afterward, the mixture was heated in an oven at 95 °C for 3 days. The white precipitate was collected by filtration, washed, and then air-dried. Finally, a calcination step was performed and the as-synthesized material was heated to 550 °C at a rate of 1−2 °C min ^{1} and kept at this temperature for 6 h to remove the templates.

Synthesis of SBA-15-apts. 1.61 mL of 3-aminopropyltriethoxysilane (apts) was added to 3 g of SBA-15 in 90 mL of toluene. This mixture was refluxed for 5 h and then filtered at room temperature. The obtained modified SBA-15-apts was then heated at 100 °C for 5 h.

Synthesis of SBA-15-apts-1 and SBA-15-apts-2. Both compounds (**NaCs-1** and **NaRb-2**) (10 wt %) were separately dissolved in water, resulting in brown solutions. While stirring, SBA-15-apts (90 wt %) was slowly added, and the solutions were kept stirring for 24 h. The solutions were then filtered and washed 3 times with water. The filtrates were colorless, indicating that both POMs were quantitatively loaded on the support. The obtained products were then collected and air-dried. Additionally, the observed decrease of the BET surface area shown in

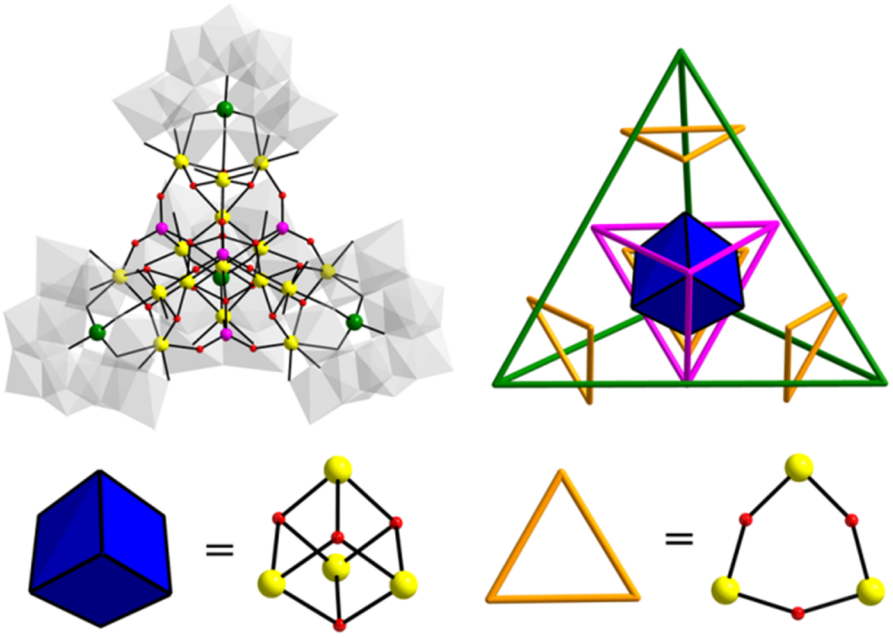

Figure 1. Top left: Combined polyhedral/ball-and-stick representation of polyanions **1** and **2**. Top right: Representation of various tetrahedral building units in **1** and **2**. Color code: WO_6 octahedra (white), Mn^{II}/Mn^{III} (yellow), P (pink), Si (green), O (red).

Table S3 is a clear indication that apts was grafted in the mesochannels of SBA-15, followed by immobilization of **1** and **2**, respectively.

X-ray Crystallography. Single crystals of **NaCs-1** and **NaRb-2** were mounted on a Hampton cryoloop in light oil for data collection at 100 K. A Bruker D8 SMART APEX II CCD diffractometer with kappa geometry and Mo−Kα radiation (graphite monochromator, $\lambda = 0.71073$ Å) was used for indexing and data collection. Data integration was performed using SAINT,[24] and routine Lorentz and polarization corrections were applied. Multiscan absorption corrections were performed using SADABS.[25] Direct methods (SHELXS97) successfully located the tungsten atoms, and successive Fourier syntheses (SHELXL2013) revealed the remaining atoms.[26] Refinements were full-matrix least-squares against $|F^2|$ using all data. In the final refinement, all non-disordered heavy atoms (Na, Cs, Rb, Mn, Si, W) were refined anisotropically; oxygen atoms and disordered counter-cations were refined isotropically. No hydrogen atoms were included in the models. Single-crystal XRD refinements showed the presence of one potassium cation in the solid lattice of **NaCs-1**, which was not detected by elemental analysis. We believe this to be a localized impurity within the crystal, as no potassium cation has been used throughout the synthesis and isolation of the product. Crystallographic data are summarized in Table S1 (Supporting Information). Further details on the crystal structure investigations may be obtained from the Fachinformationszentrum Karlsruhe, 76344 Eggenstein-Leopoldshafen,Germany (fax: (+49)7247-808-666; e-mail: crysdata@fiz-karlsruhe.de), on quoting the depository numbers 429913 (for **NaCs-1**) and 429914 (for **NaRb-2**).

XAS Measurements. The Mn $L_{2,3}$-edge X-ray absorption spectroscopy (XAS) was performed at beamline 6.3.1 of the Advanced Light Source at Lawrence Berkeley National Laboratory, USA. The spectra were taken with the sample at room temperature. Linear polarized light and total electron yield as detection mode were used.

Magnetic Susceptibility Measurements. The magnetic susceptibility measurements were obtained on a Quantum Design SQUID magnetometer MPMS-XL. This magnetometer works between 1.8 and 400 K for *dc* applied fields ranging from −7 to +7 T. Measurements were performed on polycrystalline samples. The magnetic data were corrected for the sample holder and the diamagnetic contribution.

Electrochemical Measurements. The electrochemical setup was a CHI660E driven by a PC with the CHI software. Potentials are quoted against a saturated calomel electrode (SCE). The counter electrode was a platinum gauze of large surface area. The working electrode was an ITO plate (0.3 cm^2). All experiments were performed at room temperature. The solutions were deaerated thoroughly for at least 30 min with pure argon and kept under a positive pressure of this gas during the experiments.

Catalytic Oxidation. Oxidation of cyclohexene (49 mmol, 5 mL) under a constant airflow (about 5 mL/min) and in the presence of 45 mg of catalyst (**1** and **2** supported on the modified mesoporous support SBA-15-apts) was carried out in a temperature-controlled glass vessel at 70 °C in toluene (10 mL). After the reaction, the solution was allowed to cool to room temperature and then samples were taken for GC analysis. A GC-2010 Shimadzu instrument equipped with a flame ionization detector and HP-FFAP column (50 m × 0.32 mm) was used. The carrier gas was He. The analysis of substrate loss was below 5%.

Battery Performance. The composite electrodes were prepared by mixing the active material (**NaCs-1** and **NaRb-2**, respectively), carbon black (super P), and poly(vinylidene fluoride) (PVDF) binder in a weight ratio of 60:20:20 with *N*-methylpyrrolidinone (NMP) to form a slurry. The mixture was coated onto copper foil using a doctor blade with a height of 75 mm and then dried in air at 80 °C to remove the solvent. The electrodes were roll-pressed and then punched into pieces of diameter 16 mm. These punched electrodes were dried at 110 °C under vacuum for 4 h before transferring to a glovebox. Then, the electrodes were assembled in 2016 coin cells with circular metallic lithium metal (diameter 16 mm) as counter electrode, glass fiber (Whatman, diameter 19 mm) as separator, and 1 M $LiPF_6$ in a mixture of ethylene carbonate (EC) and diethyl carbonate (DEC) (1:1 wt %) as electrolyte. Cyclic voltammetry was performed with a Biologic VMP3 potentiostat in the range of 0.01−2.0 V vs Li/Li^+ with a scan rate of 0.1 mV s^{-1}. A Neware battery tester was used for galvanostatic charge/discharge tests in the range of 0.01−2.0 V vs Li/Li^+ at a current density of 100 mA g^{-1}.

RESULTS AND DISCUSSION

Synthesis and Structure. Reaction of $Mn(OOCCH_3)_3 \cdot 2H_2O$ and $MnCl_2 \cdot 4H_2O$ with $Na_{10}[A\text{-}\alpha\text{-}SiW_9O_{34}] \cdot 23H_2O$[23] in 7:1 and 6:1 ratios, respectively, resulted in the 16-manganese-containing, mixed-valent, Keggin-based 36-tungsto-4-silicates $[Mn^{III}_{10}Mn^{II}_6O_6(OH)_6(PO_4)_4(A\text{-}\alpha\text{-}SiW_9O_{34})_4]^{28-}$ (**1**) and $[Mn^{III}_4Mn^{II}_{12}(OH)_{12}(PO_4)_4(A\text{-}\alpha\text{-}SiW_9O_{34})_4]^{28-}$ (**2**), respectively. Both reactions were carried out in aqueous medium at pH 9 and in the presence of phosphate ions. Polyanion **1** was

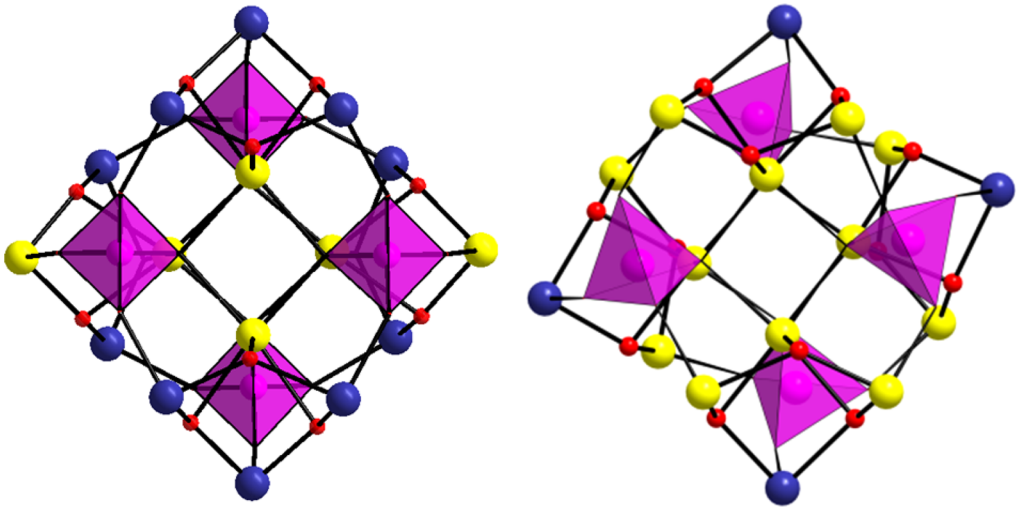

Figure 2. Ball-and-stick representation of the cationic manganese-oxo cores $\{Mn^{III}_{10}Mn^{II}_{6}O_6(OH)_6(PO_4)_4\}^{12+}$ in **1** (left) and $\{Mn^{III}_{4}Mn^{II}_{12}(OH)_{12}(PO_4)_4\}^{12+}$ in **2** (right). Color code: Mn^{II} (yellow), Mn^{III} (indigo), O (red).

isolated as the hydrated sodium-cesium salt $Na_{19.5}Cs_{8.5}[\{Mn^{III}_{10}Mn^{II}_{6}O_6(OH)_6(PO_4)_4\}(A\text{-}\alpha\text{-}SiW_9O_{34})_4]\cdot 90H_2O$ (**NaCs-1**), whereas polyanion **2** was isolated as the sodium-rubidium salt $Na_{18}Rb_{10}[Mn^{III}_{4}Mn^{II}_{12}(OH)_{12}(PO_4)_4(A\text{-}\alpha\text{-}SiW_9O_{34})_4]\cdot 75H_2O$ (**NaRb-2**). The chemical composition including counter cations and crystal waters was confirmed by elemental and thermogravimetric analyses (see the Experimental Section). Single-crystal X-ray diffraction analyses revealed that polyanions **1** and **2** crystallized in the orthorhombic *Pmmn* and monoclinic *C2/c* space groups, respectively. Both polyanions **1** and **2** are isostructural (Figure 1), each containing 16 Mn centers, but the exact number of Mn^{3+} and Mn^{2+} ions is different (see Figure 2): $10Mn^{3+}/6Mn^{2+}$ in **1** vs $4Mn^{3+}/12Mn^{2+}$ in **2** (*vide infra*). The structures of **1** and **2** comprise a central $\{Mn_4O_4\}$ cubane unit capped by four trimanganese-substituted $\{Mn_3(A\text{-}\alpha\text{-}SiW_9)\}$ Keggin units, the overall assembly being connected by four phosphate $\{PO_4\}$ linkers (Figure 1).

Bond valence sum (BVS) calculations[27] (Table S2) indicated that, for polyanion **1**, the four manganese centers in the central $\{Mn_4O_4\}$ cubane unit all have a 2+ oxidation state. In the capping $\{Mn_3(SiW_9)\}$ Keggin units, 10 out of 12 manganese ions have a 3+ oxidation state, with the 2 Mn^{2+} ions being located in two different Keggin units, which are related to each other by a mirror plane. Hence, **1** contains a total of 10 Mn^{3+} and 6 Mn^{2+} ions. Furthermore, in each $\{Mn_3(SiW_9)\}$ Keggin unit of **1**, the oxygen atoms bridging the manganese centers all have a BVS value of ca. 1.5, which we assigned as 50:50% oxo/hydroxo, resulting in a cationic $\{Mn^{III}_{10}Mn^{II}_{6}O_6(OH)_6\}^{24+}$ core, and an overall charge of 28− for polyanion **1**, which is balanced in the solid state by 19.5 sodium and 8.5 cesium counter cations, as confirmed by elemental analysis (see the Experimental Section).

BVS on polyanion **2** revealed that all four manganese centers in the central $\{Mn_4O_4\}$ cubane unit have a 2+ oxidation state, in analogy with **1**. Each of the four capping $\{Mn_3(SiW_9)\}$ units contains 1 Mn^{3+} and 2 Mn^{2+} ions, so polyanion **2** has a total of 4 Mn^{3+} and 12 Mn^{2+} ions (Table S2). All oxygen atoms bridging the manganese centers in the $\{Mn_3(SiW_9)\}$ Keggin units of **2** are monoprotonated and hence hydroxo ligands. This results in a cationic $\{Mn^{III}_{4}Mn^{II}_{12}(OH)_{12}\}^{24+}$ core, and an overall charge of 28− for polyanion **2**, which is balanced in the solid state by 18 sodium and 10 rubidium counter cations, as confirmed by elemental analysis (see the Experimental Section).

It deserves attention that the manganese-oxo clusters in **1** ($\{Mn^{III}_{10}Mn^{II}_{6}O_6(OH)_6\}^{24+}$) and **2** ($\{Mn^{III}_{4}Mn^{II}_{12}(OH)_{12}\}^{24+}$) have the exact same positive charge of 24+, in spite of different numbers of Mn^{3+} and Mn^{2+} ions, but different degrees of protonation for **1** (6 protons) and **2** (12 protons) counterbalance this effect. It is also worth noting that the $\{Mn_4O_4\}$ cubane cores in both polyanions **1** and **2** contain exclusively Mn^{2+} ions, resulting in a neutral assembly. This is fully consistent with our earlier reported $\{Co_{16}\}$ and $\{Fe_{14}Na_2\}$ analogues, which have $\{Co^{II}_{4}O_4\}$ and $\{Fe^{III}_{2}Na_2O_4\}$ cores, respectively.[20,22]

The different mixed-valence nature of polyanions **1** and **2** has structural consequences, leading to a pronounced distortion within the $\{Mn_{16}\}$ cores as well as the polyanions overall, as seen in Figure 2. Polyanion **2** displays an overall "twisted" tetrahedral arrangement, as compared to the more ideal tetrahedral one for polyanion **1**. This reduction in symmetry is also reflected in the monoclinic space group *C2/c* for **NaRb-2**, compared to the orthorhombic space group *Pmmn* for **NaCs-1**, and the former also has more IR signals, resulting in a broader spectrum (see Figure S1).

All manganese centers in **1** and **2** exhibit a distorted octahedral coordination geometry, and the respective Mn^{II}−O bond lengths are in the range of 2.066(17)−2.413(11) Å for **1** and 2.070(16)−2.463(14) Å for **2**, whereas the Mn^{III}−O bond lengths are in the range of 1.896(4)−2.325(8) Å for **1** and 1.902(15)−2.367(14) Å for **2**, which indicates the expected shorter bond lengths for manganese in the higher oxidation state. Moreover, the respective *trans* O−Mn−O bond angles are in the range of 157.9(3)−176.8(4)° for **1** and 160.7(5)−175.2(6)° for **2**, whereas the *cis* O−Mn−O bond angles are in the range of 70.0(4)−103.0(4)° for **1** and 70.6(5)−107.5(5)° for **2**.

With respect to the synthetic procedures of **1** and **2**, three points were crucial in order to successfully synthesize and isolate the desired products in best yield. First, solid Na_3PO_4 had to be added slowly to the reaction mixture, after dissolution of all other reactants, until the pH reached 9, as otherwise the yield is lower. Also, if phosphate is already present before addition of the other reagents, precipitation is induced. It seems that the presence of phosphate ions at a later stage of the reaction process directs the structural reorganization of the $\{Mn_{16}\}$ assembly, which is consistent with our previous work.[15a,20−22,28] Second, the ratio of lacunary POM precursor to manganese ions needs to be 1:7 for **1**

and 1:6 for **2** in order to obtain the highest yields, rather than the stoichiometric ratio of 1:4. Third, although both polyanions **1** and **2** contain mixed-valence (Mn^{2+}/Mn^{3+}) manganese-oxo clusters, the manganese reagents for the respective syntheses of **1** and **2** need to contain exclusively Mn^{3+} for **1** and Mn^{2+} for **2**. Any attempt to reproduce **1** and **2** by using mixtures of Mn^{2+} and Mn^{3+} salts resulted in unidentified precipitates. It should be noted that the exact number of Mn^{2+} and Mn^{3+} centers is perfectly reproducible, as we have verified by performing numerous experiments.

Synthesis of **1** with exclusively Mn^{3+} ions implies that some manganese ions must be reduced *in situ* during the course of the reaction, whereas the synthesis of **2** with exclusively Mn^{2+} ions implies that some manganese ions must be oxidized *in situ* during the course of the reaction. It should be noted that both reactions were performed in open beakers. Autoxidation and autoreduction of manganese ions in aqueous solution during reactions with lacunary POMs is not unprecedented. A literature survey on manganese-containing heteropolytungstates demonstrated several examples of mixed-valence manganese centers in the final products, with manganese in a single oxidation state being used in the reactions.[8j,10d,14] However, preformed mixed-valence, multinuclear manganese complexes have also been used for the synthesis of mixed-valence Mn-containing POMs.[7d,e,g,8h,k] Finally, the isolation process of polyanions **1** and **2** as bulk pure crystalline solids in maximum yields required the presence of cesium ions in the case of **1** and rubidium ions for **2**.

XAS Measurements. X-ray absorption spectra on **NaCs-1** and **NaRb-2** were carried out at room temperature using beamline 6.3.1 of the Advanced Light Source for linear polarized light with total electron yield as detection mode. The spectra were compared with those of the reference compounds $[Mn^{II}_4(C_{12}H_9N_2O)_6](BF_4)_2{\cdot}2CH_3CN{\cdot}H2O$ ("MnStar", only Mn^{2+}-containing)[29] and $[Mn^{III}_6(\mu_3\text{-}O)_2(Salox)_6(CH_3CH_2OH)_4\{(CH_3)_3CCOO\}_2]$ ("Mn salox", only Mn^{3+}-containing);[30] see Figure 3.

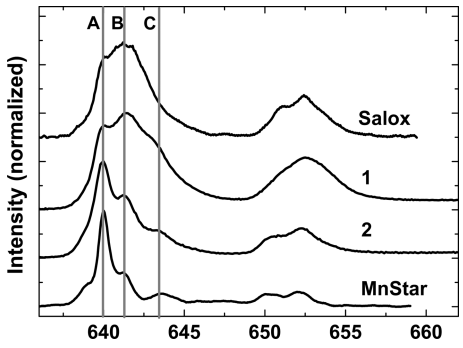

Figure 3. Manganese $L_{2,3}$-edge X-ray absorption spectra of **NaCs-1** and **NaRb-2**. For comparison, the spectra of the exclusively Mn^{2+}-containing "MnStar"[29] and the exclusively Mn^{3+}-containing "Salox"[30] are also displayed.

The Mn L_3 edge of MnStar comprises three distinct features, namely, an absolute maximum of absorption at 640 eV (labeled A), and shoulders around 641.5 eV (B), and 643.5 eV (C), whereas the L_3 X-ray absorption of Salox peaks at 641.5 eV (B) (Figure 3). The Mn XAS of Salox also shows a feature around 640 eV, which can be attributed to charge transfer excitations (d5L states). The L_2 edge (spanning the range of ~650−655 eV) of MnStar comprises two small, but rather sharp, peaks. In contrast, the Mn L_2 edge of Salox consists of a rather broad multiplet structure and less sharp features. The Mn $L_{2,3}$-edge XAS of **NaRb-2** has its absolute maximum in intensity at 640 eV (A), confirming that the major fraction of the Mn ions in **2** is divalent. However, feature B, corresponding to the Salox L_3 edge maximum is significantly more pronounced compared to MnStar, indicating also the presence of trivalent Mn ions in **2**. In contrast, the Mn L_3 multiplet structure of **NaCs-1** is more similar to the spectrum of Salox, confirming that the majority of the Mn ions in **1** are in a trivalent state. However, a more intense feature A and the presence of a significant feature C as compared to Salox suggest that also some divalent Mn ions are present in **1**.

Magnetic Measurements. Temperature-dependent *dc* magnetic susceptibility measurements were carried out on solid samples of polyanions **1** and **2** in the temperature range 1.8−300 K in a field of 1000 Oe (Figure 4).

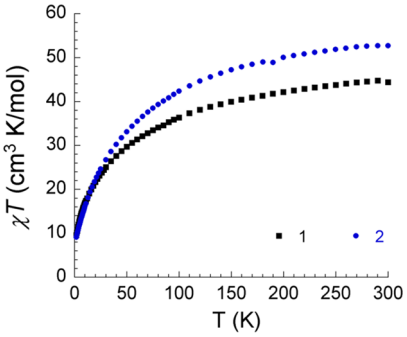

Figure 4. Temperature dependence of the χT product for polycrystalline samples of **1** (squares) and **2** (circles) at 1000 Oe.

The $_{\chi M}T$ value of polyanion **1** progressively decreases from 44.7 cm^3 K mol^{-1} at 300 K to 22.8 cm^3 K mol^{-1} at ~40 K before falling rapidly to 9.6 cm^3 K mol^{-1} at 1.8 K. For polyanion **2**, the $_{\chi M}T$ values decrease from 52.8 cm^3 K mol^{-1} at 300 K to 8.9 cm^3 K mol^{-1} at 1.8 K. The spin-only $_{\chi M}T$ value for polyanion **1** comprising 10 noninteracting Mn^{3+} and 6 Mn^{2+} ions is 56.25 cm^3 K mol^{-1}, and for polyanion **2** comprising 4 Mn^{3+} and 12 Mn^{2+} ions is 64.50 cm^3 K mol^{-1}, and hence, Figure 4 is indicative of an appreciable antiferromagnetic exchange between the Mn^{3+} and Mn^{2+} centers in **1** and **2**. For polyanions **1** and **2**, the total spin value ranges would vary from 0 to 35 and from 0 to 38, respectively. To determine their spin ground states, magnetization data were collected in the temperature range 2−5 K and in the magnetic field range 0−70000 Oe (Figure S4). The magnetization data for both compounds do not show any saturation even at the highest field measured. Possible reasons could be the presence of magnetic spin frustration or significant zero-field splitting in the spin ground state. Low-lying excited states are also anticipated for such big ions which generally have a high density of molecular spin states.

Also, *ac* susceptibility measurements were carried out in zero and nonzero *dc* fields, but no peaks down to 1.8 K and no frequency-dependent in-phase and out-of-phase signals were observed (Figures S5 and S6). The latter results indicate that polyanions **1** and **2** are not single-molecule magnets.

Electrochemistry. The redox behavior of **1** and **2** was studied in pH 7 media. The UV−visible stability carried out in these media revealed that both polyanions are sufficiently stable to stand electrochemical characterization (see the SI for details). Ever since the pioneering work of Pope and co-workers,[6a,8c,31a,b] numerous examples were reported on the electrochemical generation of high-valent manganese center(s) within poly-

oxotungstates.[6e,7d−g,13,16,18a,b,19,31c−f] These redox processes are well-known to depend on various parameters including solvent, pH, and composition of electrolyte.[31c,d,f] The electrochemical generation of higher-valent multinuclear manganese complexes is an important issue because most of them can act as earth-abundant metal electrocatalysts for several challenging oxidation processes including the oxygen-evolving reaction (OER).[7e,16,19,31c,e] Figure 5A shows the redox activity of the

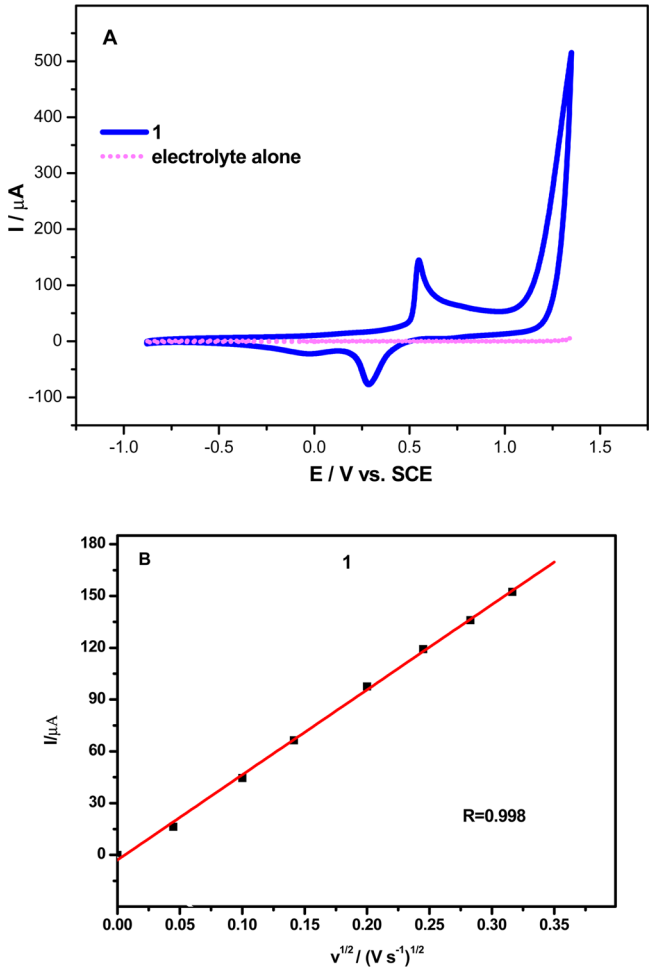

Figure 5. Redox activity of the Mn^{3+} and Mn^{4+} centers of 50 μM **1** in a pH 7 medium (1 M $LiCH_3COO/CH_3COOH$). The scan rate was 100 mV s^{-1}, and the reference electrode was a saturated calomel electrode (SCE). (A) Dotted pink line: background current; full blue line: cyclic voltammogram recorded in the presence of **1**. (B) Variation of the Mn oxidation peak current intensity as a function of the square root of the scan rate.

Mn centers of 50 μM **1** and that of the supporting electrolyte alone between −0.880 and +1.350 V versus SCE at a scan rate of 100 mV s^{-1}. The reduction of the Mn^{3+} centers to Mn^{2+} is represented by a broad wave peaking at −0.040 V versus SCE. On the reverse scan, the CV pattern features one quasi-reversible oxidation wave (at +0.548 V versus SCE) preceded by a low intensity prewave and followed by a large irreversible wave. In agreement with previous reports, these waves are assigned to the stepwise oxidation of Mn^{2+} to Mn^{4+} and the OER, respectively.[7e,16,31e] The rereduction of the Mn^{4+} centers to Mn^{3+} is also featured by a well-defined wave located at +0.286 V vs SCE. The remarkable outcome is that the presence of **1** makes it perfectly possible to observe the OER wave in a potential region where appreciable oxidation current does not appear on the CV recorded with the electrolyte alone. The variation of the Mn oxidation peak current as a function of the square root of the potential scan rate is shown in Figure 5B. The linearity of this curve demonstrates that the CVs feature a diffusion-controlled process. The Mn centers redox processes and the OER associated with **2** are also featured by well-behaved waves (Figure S8), but the oxidation potential of Mn^{2+} to Mn^{4+} in **2** is shifted in the positive direction (by 0.070 V) compared to **1**, which means that the latter is slightly easier to oxidize. It is worth noting that reaching the OER wave has no deleterious effect on the redox processes associated with the Mn and W centers. However, the determination of the nature of the true electrocatalyst and the study of its stability during the OER are among the main challenges and will be investigated in the future.

The W^{6+} centers in **1** and **2** exhibit two quasi-reversible and well-defined reduction waves with the same general shape (Figure 6).

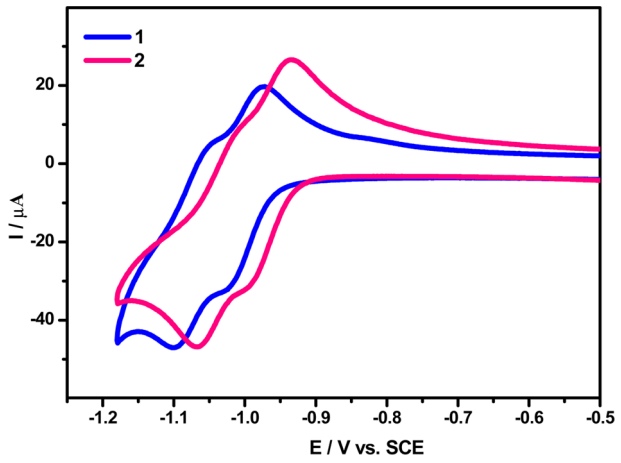

Figure 6. Cyclic voltammograms of the quasi-reversible W^{6+} waves of **1** and **2**, respectively, run in a pH 7 (1 M Li CH_3COO + CH_3COOH) medium. The scan rate was 100 mV s^{-1}, and the reference electrode was a saturated calomel electrode (SCE). The concentration of the polyanions was 50 μM.

However, when compared to **1**, a slight anodic shift of ca. 0.035 V was observed for both W reduction waves of **2** (at ca. −0.993 and −1.067 V vs SCE, respectively). It is well-known that the voltammetric behaviors of most POMs depend on several parameters including the basicity of the reduced species and, occasionally, of the fully oxidized species.[32] The overpotential required for the onset of the OER (425 mV) is lower than that observed for $[Mn^{III}{}_3Mn^{IV}O_3(CH_3COO)_3(A\text{-}\alpha\text{-}SiW_9O_{34})]^{6-}$ (530 mV),[19] but the smallest value reported for a manganese-containing POM was observed for $[Mn_{19}(OH)_{12}(SiW_{10}O_{37})_6]^{34-}$ (330 mV).[16] It is worth noting that the electrolytes used in these reports are more acidic (pH 5) compared with the pH 7 medium used here. Therefore, polyanion **1** is potentially a good candidate for efficient electrocatalysis of the OER.

Catalysis. The heterogeneous catalytic activity of **1** and **2** for cyclohexene oxidation was carried out by loading both polyanions on a modified mesoporous support of SBA-15-apts (see details in the Experimental Section).[33] The BET surface area of these supported catalysts was measured and determined to be around 350 m^2/g (Table S3; see the SI). According to our experiments, the desired reaction (Scheme 1) did not occur in

the blank test without any catalyst or in the presence of the support alone, whether SBA-15 or SBA-15-apts.

Scheme 1. Cyclohexene Allylic Oxidation Pathway

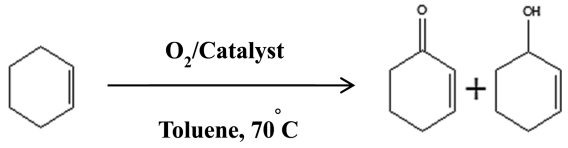

The homogeneous and heterogeneous catalytic oxidation of cyclohexene has been previously studied with several transition metal-modified mesoporous materials and various transition metal-containing POMs (including manganese) under different oxidizing conditions, where the product distribution varied accordingly.[34] In some cases, the corresponding epoxide of cyclohexene dominated, whereas the allylic products did in other cases.

Here, the selectivity toward 2-cyclohexene-1-one was higher than that toward 2-cyclohexene-1-ol, reaching a maximum of 52−55% and 32−38%, respectively. Such product distribution, where allylic oxidation products are dominant, is typical for a homolytic oxidation mechanism.[34e,f]

As shown in Table 1, cyclohexene conversion increased from 50% to 63% when **2** was used as a catalyst instead of **1**, and the

Table 1. Air Oxidation of Cyclohexene by Polyanions 1 and 2 Immobilized on SBA-15-apts[a]

		selectivity (%)[b,c]		
catalyst	(%) conv. cyclohexene	allylic ketone	allylic alcohol	TOF (h^{-1})[d]
SBA-15-apts-1	50	55.5	32.4	3100
SBA-15-apts-2	63	52.26	38.4	3740

[a]Reaction conditions: cyclohexene (49 mmol, 5 mL), toluene (10 mL), catalyst amount: 45 mg, 70 °C, 24 h, airflow: 5 mL/min. [b]GC yield based on cyclohexene consumed. [c]Some other unidentified products up to 12%. [d]TOF = (moles of consumed cyclohexene)/(moles of POM × time).

former also has a higher turnover frequency (TOF) than the latter (3740 h^{-1} vs 3100 h^{-1}). It appears that not only the total number and oxidation state of the manganese centers is important, but also the detailed structural arrangement of these metal ions in the polyanion structure. It should be remembered that the number of Mn^{3+} and Mn^{2+} ions is different in polyanions **1** and **2**, and the latter also exhibits a small structural distortion (see Figure 2), compared to the more ideal tetrahedral situation for **1**.

Battery Performance. We decided to test the concept of **NaCs-1** and **NaRb-2** as anode materials in lithium ion battery (LIB) applications. The battery performances were investigated by galvanostatic charge−discharge (GCD) cycling and cyclic voltammetry (CV) in a half-cell configuration as described in the Experimental Section. CVs were measured for the first three cycles at a scan rate of 0.1 mV s^{-1} over a potential range of 0.01−2.0 V vs Li/Li^+ in order to understand the electrochemical properties of **NaCs-1** and **NaRb-2** electrodes, as shown in Figure 7A,B. The **NaCs-1** and **NaRb-2** electrodes exhibited similar behavior in the CV curves. The solid electrolyte interphase (SEI) formed in the first cycle and generated an irreversible reduction peak at ∼0.7 V vs Li/Li^+ which disappeared in the following cycles.[3d] The main oxidation peaks can be observed at 1.07 and 0.17 V vs Li/Li^+, and the corresponding reduction peaks are located at 0.30 and 0.01 V vs Li/Li^+. These peaks might result from the redox transition of Mn and W, and the insertion/extraction of Li ions with good reversibility. This can be further proven by X-ray photoelectron spectroscopy (XPS) and in situ X-ray absorption spectroscopy (XAS), which are not discussed here.

Figure 7C,D shows the galvanostatic charge−discharge (GCD) curves of the **NaCs-1** and **NaRb-2** electrodes with initially 2 cycles at a current density of 100 mA g^{-1}. Two well-defined plateaus can be observed on the discharge/charge curves where the potentials of the plateaus are similar to the redox peaks in the CV curves. The discharge capacity of the **NaCs-1** and **NaRb-2** electrodes in the first cycle are 908 and 727 mAh g^{-1}, and the discharge capacities in the second cycle are 430 and 316 mAh g^{-1}, respectively. These results are comparable with graphite (theoretical capacity: 372 mAh g^{-1}), which is the most commonly used anode material in LIBs.[35]

The **NaCs-1** and **NaRb-2** electrodes exhibit high cycling stability with excellent Coulombic efficiencies of ∼100% up to 50 cycles; see Figure 7E,F. The capacity retention for the **NaCs-1** electrode is 77% and for the **NaRb-2** electrode is 85% (calculated using discharge capacity from 2nd to 50th cycle). The above results suggest that **NaCs-1** and **NaRb-2** electrodes are potentially interesting anode materials for real LIB applications.

CONCLUSIONS

We have successfully synthesized the two 16-manganese-containing 36-tungsto-4-silicates $[Mn^{III}_{10}Mn^{II}_{6}O_6(OH)_6(PO_4)_4(A\text{-}\alpha\text{-}SiW_9O_{34})_4]^{28-}$ (**1**) and $[Mn^{III}_{4}Mn^{II}_{12}(OH)_{12}(PO_4)_4(A\text{-}\alpha\text{-}SiW_9O_{34})_4]^{28-}$ (**2**) by careful tuning of the synthetic conditions. Interestingly, polyanions **1** and **2** comprise mixed-valent, cationic $\{Mn^{III}_{10}Mn^{II}_{6}O_6(OH)_6\}^{24+}$ and $\{Mn^{III}_{4}Mn^{II}_{12}(OH)_{12}\}^{24+}$ cores, respectively, which have exactly the same charge. Synthesis of **1** and **2** using exclusively Mn^{3+} and Mn^{2+} ions, respectively, implies autoxidation and autoreduction of manganese ions *in situ*. The hydrated mixed alkali salts of **1** and **2** were investigated in the solid state by single-crystal X-ray diffraction, FT-IR spectroscopy, thermogravimetric and elemental analyses, as well as X-ray absorption spectroscopy. Magnetic studies showed that polyanions **1** and **2** do not act as molecular magnets and possess a complex spin ground state which does not saturate even at 70000 Oe. Both **1** and **2** enhance the OER as shown by electrochemistry, and they also act as heterogeneous catalysts in the oxidation of cyclohexene. The difference in activity can be related to the different numbers of Mn^{3+} and Mn^{2+} ions and possibly a resulting subtle structural variation and warrants further investigation. Furthermore, both **1** and **2** have been shown to act as potential anode candidates for LIBs with an initial discharge capacity of 908 and 727 mAh g^{-1}, respectively, and excellent Coulombic efficiencies ∼ 100% up to 50 cycles.

In summary, we have expanded the class of M_{16}-containing tetrahedral polyanions to manganese with the discovery of two isostructural, mixed-valent $Mn^{2+/3+}$ derivatives. Such compounds are structurally appealing, but more importantly, they contain a multitude of interesting electronic, redox, magnetic, and catalytic properties, which we have all explored. In future work, we plan to investigate the catalytic properties of **1** and **2** in more detail, including water oxidation, and we will also try expanding this POM class further structurally and compositionally.

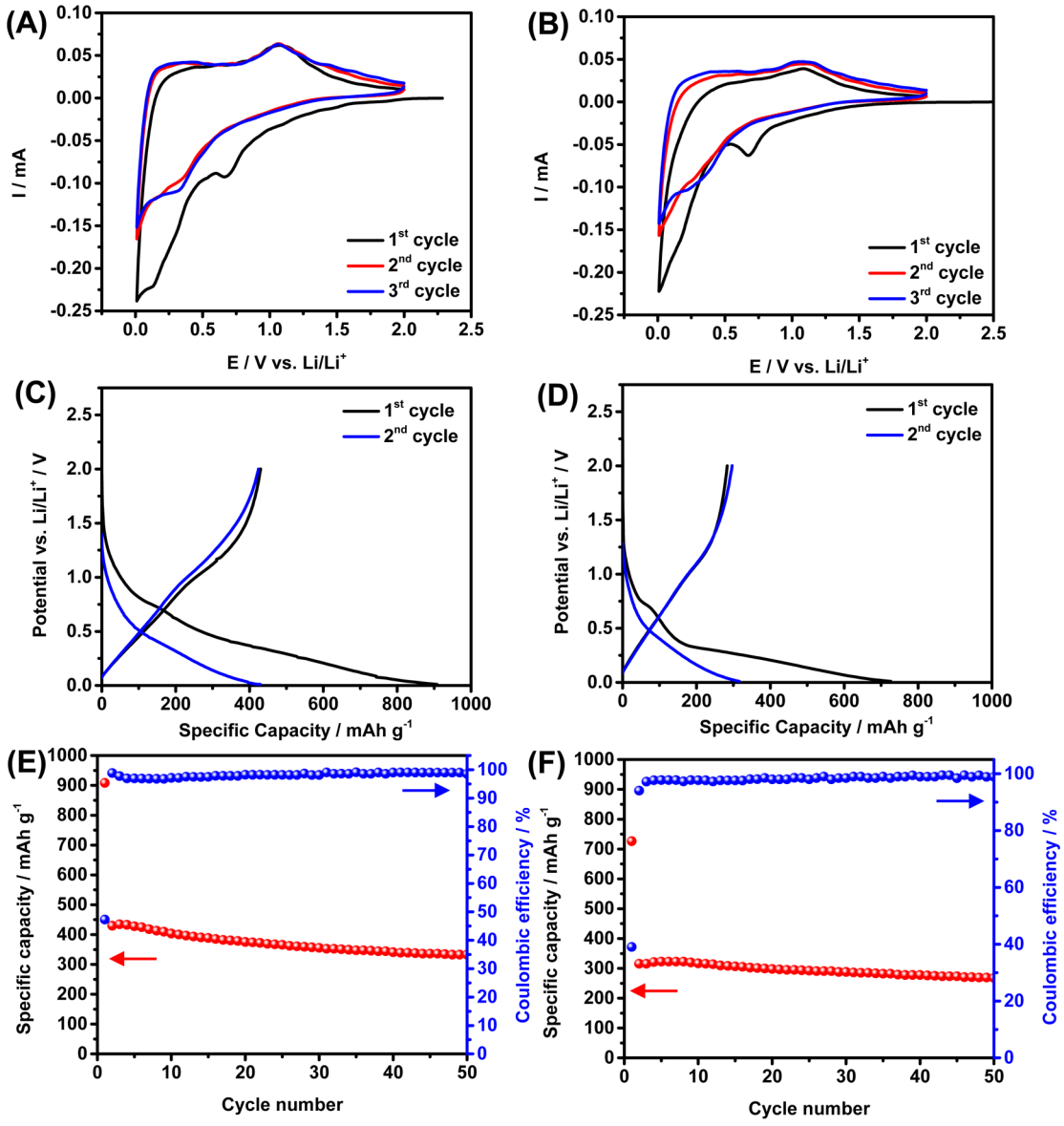

Figure 7. Battery performance of electrodes based on **1** and **2** in 1 M $LiPF_6$/EC:DEC (1:1) in a half-cell configuration with Li metal as counter electrode: cyclic voltammograms of (a) **NaCs-1** and (b) **NaRb-2** electrodes measured at a scan rate of 0.1 mV s^{-1}; the galvanostatic charge−discharge curves of (c) **NaCs-1** and (d) **NaRb-2** electrodes measured at a current density of 100 mA g^{-1}; the cycling performance and the Coulombic efficiency of (e) **NaCs-1** and (f) **NaRb-2** electrodes measured at a current density of 100 mA g^{-1}.

AUTHOR INFORMATION

Corresponding Author

*E-mail: u.kortz@jacobs-university.de. Fax: (+49)421-200-3102. Homepage: www.jacobs-university.de/ses/ukortz.

Present Address

☆Institute of Nanotechnology, Karlsruhe Institute of Technology (KIT), Hermann-von-Helmholtz Platz 1, 76344 Eggenstein-Leopoldshafen, Germany.

Author Contributions

□A.H. and M.I. contributed equally to this work.

Notes

The authors declare no competing financial interest.

△B.K. is retired.

ACKNOWLEDGMENTS

U.K. thanks the German Science Foundation (DFG, KO 2288/20-1), the CMST COST Action CM1203 (PoCheMoN), and Jacobs University for research support, and kindly acknowledges the Chinese Academy of Sciences President's International Fellowship Initiative (Grant No. 2015VMA041). A.H. thanks DAAD for a doctoral fellowship. M.I. thanks DFG and Institute

of Nanotechnology, Karlsruhe Institute of Technology (KIT), for a postdoctoral fellowship, and she also thanks DAAD and the Higher Education Commission of Pakistan for a doctoral fellowship (Jacobs University). She also acknowledges the University of Balochistan, Quetta, Pakistan, for allowing her to pursue Ph.D. (Jacobs University) and postdoctoral (KIT) studies in Germany. The Advanced Light Source is supported by the Director, Office of Science, Office of Basic Energy Sciences, of the U.S. Department of Energy, under Contract No. DE-AC02-05CH11231. G.Z. thanks the National Science Foundation of China (No. 21371173) for the funding and research support. H.-Y.C. and U.S. thank TUM CREATE, National Research Foundation of Singapore, and Newcastle University for research and funding support. Figures 1 and 2 were generated by Diamond, Version 3.2 (copyright Crystal Impact GbR).

REFERENCES

(1) (a) Pope, M. T. *Heteropoly and Isopoly Oxometalates*; Springer: Berlin, 1983. (b) Cronin, L. In *Comprehensive Coordination Chemistry II*; McCleverty, J. A., Meyer, T. J., Eds.; Elsevier: Amsterdam, 2004; Vol. 7, pp 1−56. (c) Pope, M. T.; Kortz, U. Polyoxometalates. In *Encyclopedia of Inorganic and Bioinorganic Chemistry*; John Wiley & Sons, Ltd.: Hoboken, NJ, 2012.

(2) (a) Pope, M. T.; Müller, A. *Angew. Chem., Int. Ed. Engl.* **1991**, *30*, 34−48. (b) Hill, C. L.; Prosser-McCartha, C. M. *Coord. Chem. Rev.* **1995**, *143*, 407−455. (c) *Chem. Rev.* **1998**, *98*, 1, 1−390. Special Issue on Polyoxometalates. 10.1021/cr960395y. (d) Müller, A.; Roy, S. *Coord. Chem. Rev.* **2003**, *245*, 153−166. (e) Hasenknopf, B.; Micoine, K.; Lacôte, E.; Thorimbert, S.; Malacria, M.; Thouvenot, R. *Eur. J. Inorg. Chem.* **2008**, *2008*, 5001−5013. (f) Kortz, U.; Müller, A.; van Slageren, J.; Schnack, J.; Dalal, N. S.; Dressel, M. *Coord. Chem. Rev.* **2009**, *253*, 2315−2327. (g) *Eur. J. Inorg. Chem.* **2009**, *2009*, 34, 5055−5276. Special Issue: Polyoxometalates. (h) Long, D. L.; Tsunashima, R.; Cronin, L. *Angew. Chem., Int. Ed.* **2010**, *49*, 1736−1758. (i) Izarova, N. V.; Pope, M. T.; Kortz, U. *Angew. Chem., Int. Ed.* **2012**, *51*, 9492−9510. (j) Clemente-Juan, J. M.; Coronado, E.; Gaita-Ariño, A. *Chem. Soc. Rev.* **2012**, *41*, 7464−7478. (k) Lv, H.; Geletii, Y. V.; Zhao, C.; Vickers, J. W.; Zhu, G.; Luo, Z.; Song, J.; Lian, T.; Musaev, D. G.; Hill, C. L. *Chem. Soc. Rev.* **2012**, *41*, 7572−7589.

(3) (a) Chen, H.−Y.; Al-Oweini, R.; Friedl, J.; Lee, C. Y.; Li, L.; Kortz, U.; Stimming, U.; Srinivasan, M. *Nanoscale* **2015**, *7*, 7934−7941. (b) Hartung, S.; Bucher, N.; Chen, H. − Y.; Al-Oweini, R.; Sreejith, S.; Borah, P.; Yanli, Z.; Kortz, U.; Stimming, U.; Hoster, H.; Srinivasan, M. *J. Power Sources* **2015**, *288*, 270−277. (c) Chen, H.-Y.; Wee, G.; Al-Oweini, R.; Friedl, J.; Tan, K. S.; Wang, Y.; Wong, C. L.; Kortz, U.; Stimming, U.; Srinivasan, M. *ChemPhysChem* **2014**, *15*, 2162−2169. (d) Ma, D.; Liang, L.; Chen, W.; Liu, H.; Song, Y.-F. *Adv. Funct. Mater.* **2013**, *23*, 6100−6105.

(4) (a) *Chem. Soc. Rev.* **2012**, *41*, 22, 7325−7648. Themed Issue: Polyoxometalate Cluster Science. (b) Zheng, S. T.; Yang, G. Y. *Chem. Soc. Rev.* **2012**, *41*, 7623−7646. (c) Oms, O.; Dolbecq, A.; Mialane, P. *Chem. Soc. Rev.* **2012**, *41*, 7497−7536.

(5) (a) Lyon, D. K.; Miller, W. K.; Novet, T.; Domaille, P. J.; Evitt, E.; Johnson, D. C.; Finke, R. G. *J. Am. Chem. Soc.* **1991**, *113*, 7209−7221. (b) Cowan, J. J.; Bailey, A. J.; Heintz, R. A.; Do, B. T.; Hardcastle, K. I.; Hill, C. L.; Weinstock, I. A. *Inorg. Chem.* **2001**, *40*, 6666−6675. (c) Bassil, B. S.; Dickman, M. H.; Reicke, M.; Kortz, U.; Keita, B.; Nadjo, L. *Dalton Trans.* **2006**, 4253−4259. (d) Zhang, D.; Zhang, Y.; Zhao, J.; Ma, P.; Wang, J.; Niu, J. *Eur. J. Inorg. Chem.* **2013**, *2013*, 1672−1680. (e) Sato, R.; Suzuki, K.; Minato, T.; Shinoe, M.; Yamaguchi, K.; Mizuno, N. *Chem. Commun.* **2015**, *51*, 4081−4084.

(6) (a) Zhang, X. Y.; O'Connor, C. J.; Jameson, G. B.; Pope, M. T. *Inorg. Chem.* **1996**, *35*, 30−34. (b) Kortz, U.; Al-Kassem, N. K.; Savelieff, M. G.; Al Kadi, N. A.; Sadakane, M. *Inorg. Chem.* **2001**, *40*, 4742−4749. (c) Zhang, Z. M.; Yao, S.; Li, Y. G.; Wang, Y. H.; Qi, Y. F.; Wang, E. B. *Chem. Commun.* **2008**, 1650−1652. (d) Hou, Y.; Xu, L.; Cichon, M. J.; Lense, S.; Hardcastle, K. I.; Hill, C. L. *Inorg. Chem.* **2010**, *49*, 4125−4132. (e) Car, P. E.; Spingler, B.; Weyeneth, S.; Patscheider, J.; Patzke, G. R. *Polyhedron* **2013**, *52*, 151−158. (f) Jiao, Y. Q.; Qin, C.; Wang, X. L.; Liu, F. H.; Huang, P.; Wang, C. G.; Shao, K. Z.; Su, Z. M. *Chem. Commun.* **2014**, *50*, 5961−5963. (g) Winter, R. S.; Long, D. L.; Cronin, L. *Inorg. Chem.* **2015**, *54*, 4151−4155.

(7) (a) Liu, J. G.; Ortéga, F.; Sethuraman, P.; Katsoulis, D. E.; Costello, C. E.; Pope, M. T. *J. Chem. Soc., Dalton Trans.* **1992**, 1901−1906. (b) Kortz, U.; Matta, S. *Inorg. Chem.* **2001**, *40*, 815−817. (c) Mialane, P.; Marrot, J.; Riviére, E.; Nebout, J.; Hervé, G. *Inorg. Chem.* **2001**, *40*, 44−48. (d) Dutta, D.; Jana, A. D.; Debnath, M.; Mostafa, G.; Clérac, R.; Tojal, J. G.; Ali, M. *Eur. J. Inorg. Chem.* **2010**, *2010*, 5517−5522. (e) Al-Oweini, R.; Bassil, B. S.; Palden, T.; Keita, B.; Lan, Y.; Powell, A. K.; Kortz, U. *Polyhedron* **2013**, *52*, 461−466. (f) Shevchenko, D.; Huang, P.; Bon, V. V.; Anderlund, M. F.; Kokozay, V. N.; Styring, S.; Thapper, A. *Dalton Trans.* **2013**, *42*, 5130−5139. (g) Al-Oweini, R.; Bassil, B. S.; Friedl, J.; Kottisch, V.; Ibrahim, M.; Asano, M.; Keita, B.; Novitchi, G.; Lan, Y.; Powell, A. K.; Stimming, U.; Kortz, U. *Inorg. Chem.* **2014**, *53*, 5663−5673.

(8) (a) Gomez-Garcia, C. J.; Coronado, E.; Gomez-Romero, P.; Casan-Pastor, N. *Inorg. Chem.* **1993**, *32*, 3378−3381. (b) Gomez-Garcia, C. J.; Borras-Almenar, J. J.; Coronado, E.; Ouahab, L. *Inorg. Chem.* **1994**, *33*, 4016−4022. (c) Zhang, X.-Y.; Jameson, G. B.; O' Connor, C. J.; Pope, M. T. *Polyhedron* **1996**, *15*, 917−922. (d) Bi, L. H.; Wang, E. B.; Peng, J.; Huang, R. D.; Xu, L.; Hu, C. W. *Inorg. Chem.* **2000**, *39*, 671−679. (e) Kortz, U.; Isber, S.; Dickman, M. H.; Ravot, D. *Inorg. Chem.* **2000**, *39*, 2915−2922. (f) Kortz, U.; Nellutla, S.; Stowe, A. C.; Dalal, N. S.; Rauwald, U.; Danquah, W.; Ravot, D. *Inorg. Chem.* **2004**, *43*, 2308−2317. (g) Mialane, P.; Duboc, C.; Marrot, J.; Rivière, E.; Dolbecq, A.; Sécheresse, F. *Chem.—Eur. J.* **2006**, *12*, 1950−1959. (h) Fang, X. K.; Speldrich, M.; Schilder, H.; Cao, R.; O' Halloran, K. P.; Hill, C. L.; Kögerler, P. *Chem. Commun.* **2010**, *46*, 2760−2765. (i) Bassil, B. S.; Ibrahim, M.; Mal, S. S.; Suchopar, A.; Biboum, R. N.; Keita, B.; Nadjo, L.; Nellutla, S.; van Tol, J.; Dalal, N. S.; Kortz, U. *Inorg. Chem.* **2010**, *49*, 4949−4959. (j) Yao, S.; Yan, J.; Yu, Y.; Wang, E. *J. Coord. Chem.* **2012**, *65*, 1451−1458. (k) Fang, X.; McCallum, K.; Pratt, H. D., III; Anderson, T. M.; Dennis, K.; Luban, M. *Dalton Trans.* **2012**, *41*, 9867−9870.

(9) Suzuki, K.; Sato, R.; Minato, T.; Shinoe, M.; Yamaguchi, K.; Mizuno, N. *Dalton Trans.* **2015**, *44*, 14220−14226.

(10) (a) Ritorto, M. D.; Anderson, T. M.; Neiwert, W. A.; Hill, C. L. *Inorg. Chem.* **2004**, *43*, 44−49. (b) Ritchie, C.; Ferguson, A.; Nojiri, H.; Miras, H. N.; Song, Y. F.; Long, D. L.; Burkholder, E.; Murrie, M.; Kögerler, P.; Brechin, E. K.; Cronin, L. *Angew. Chem., Int. Ed.* **2008**, *47*, 5609−5612. (c) Mitchell, S. G.; Khanra, S.; Miras, H. N.; Boyd, T.; Long, D. L.; Cronin, L. *Chem. Commun.* **2009**, 2712−2714. (d) Jiang, N.; Li, F. Y.; Xu, L.; Li, Y. G.; Li, J. M. *Inorg. Chem. Commun.* **2010**, *13*, 372−375. (e) Mitchell, S. G.; Molina, P. I.; Khanra, S.; Miras, H. N.; Prescimone, A.; Cooper, G. J. T.; Winter, R. S.; Brechin, E. K.; Long, D. L.; Cogdell, R. J.; Cronin, L. *Angew. Chem., Int. Ed.* **2011**, *50*, 9154−9157. (f) Yang, L.; Liu, Q.; Ma, P.; Niu, J.; Wang, J. *Dalton Trans.* **2015**, *44*, 13469−13472.

(11) (a) Nsouli, N. H.; Ismail, A. H.; Helgadottir, I. S.; Dickman, M. H.; Clemente-Juan, J. M.; Kortz, U. *Inorg. Chem.* **2009**, *48*, 5884−5890. (b) Chen, L. J.; Shi, D. Y.; Zhao, J. W.; Wang, Y. L.; Ma, P. T.; Wang, J. P.; Niu, J. Y. *Cryst. Growth Des.* **2011**, *11*, 1913−1923. (c) Fang, X. K.; Kögerler, P.; Speldrich, M.; Schilder, H.; Luban, M. *Chem. Commun.* **2012**, *48*, 1218−1220. (d) Winter, R. S.; Yan, J.; Busche, C.; Mathieson, J. S.; Prescimone, A.; Brechin, E. K.; Long, D. L.; Cronin, L. *Chem.—Eur. J.* **2013**, *19*, 2976−2981.

(12) (a) Huang, L.; Cheng, L.; Fang, W. H.; Wang, S. S.; Yang, G. Y. *Eur. J. Inorg. Chem.* **2013**, *2013*, 1693−1698. (b) Molina, P. I.; Miras, H. N.; Long, D. L.; Cronin, L. *Inorg. Chem.* **2013**, *52*, 9284−9289.

(13) Mitchell, S. G.; Miras, H. N.; Long, D. L.; Cronin, L. *Inorg. Chim. Acta* **2010**, *363*, 4240−4246.

(14) Zhang, Z. M.; Yao, S.; Li, Y. G.; Wu, H. H.; Wang, Y. H.; Rouzières, M.; Clérac, R.; Su, Z. M.; Wang, E. B. *Chem. Commun.* **2013**, *49*, 2515−2517.

(15) (a) Wu, Q.; Li, Y. G.; Wang, Y. H.; Wang, E. B.; Zhang, Z. M.; Clérac, R. *Inorg. Chem.* **2009**, *48*, 1606−1612. (b) Fang, X. K.; Luban, M. *Chem. Commun.* **2011**, *47*, 3066−3068.

(16) Bassil, B. S.; Ibrahim, M.; Al-Oweini, R.; Asano, M.; Wang, Z. X.; van Tol, J.; Dalal, N. S.; Choi, K. Y.; Biboum, R. N.; Keita, B.; Nadjo, L.; Kortz, U. *Angew. Chem., Int. Ed.* **2011**, *50*, 5961−5964.
(17) Fang, X.; Kögerler, P.; Furukawa, Y.; Speldrich, M.; Luban, M. *Angew. Chem., Int. Ed.* **2011**, *50*, 5212−5216.
(18) (a) Mbomekalle, I. M.; Keita, B.; Nierlich, M.; Kortz, U.; Berthet, P.; Nadjo, L. *Inorg. Chem.* **2003**, *42*, 5143−5152. (b) Mbomekalle, I. M.; Keita, B.; Nadjo, L.; Neiwert, W. A.; Zhang, L.; Hardcastle, K. I.; Hill, C. L.; Anderson, T. M. *Eur. J. Inorg. Chem.* **2003**, *2003*, 3924−3928. (c) Keita, B.; Mbomekallé, I. M.; Nadjo, L.; Anderson, T. M.; Hill, C. L. *Inorg. Chem.* **2004**, *43*, 3257−3263. (d) Ruhlmann, L.; Costa-Coquelard, C.; Canny, J.; Thouvenot, R. *Eur. J. Inorg. Chem.* **2007**, *2007*, 1493−1500. (e) Fang, X. F.; Kögerler, P. *Angew. Chem., Int. Ed.* **2008**, *47*, 8123−8126. (f) Fang, X. K.; Kögerler, P. *Chem. Commun.* **2008**, 3396−3398. (g) Reinoso, S.; Gálán-Mascarós, J. R. *Inorg. Chem.* **2010**, *49*, 377−379.
(19) Al-Oweini, R.; Sartorel, A.; Bassil, B. S.; Natali, M.; Berardi, S.; Scandola, F.; Kortz, U.; Bonchio, M. *Angew. Chem., Int. Ed.* **2014**, *53*, 11182−11185.
(20) (a) Ibrahim, M.; Lan, Y.; Bassil, B. S.; Xiang, Y.; Suchopar, A.; Powell, A. K.; Kortz, U. *Angew. Chem., Int. Ed.* **2011**, *50*, 4708−4711. (b) Ibrahim, M.; Haider, A.; Lan, Y.; Bassil, B. S.; Carey, A. M.; Liu, R.; Zhang, G.; Keita, B.; Li, W.; Kostakis, G. E.; Powell, A. K.; Kortz, U. *Inorg. Chem.* **2014**, *53*, 263−266.
(21) Han, X. B.; Zhang, Z. M.; Zhang, T.; Li, Y. G.; Lin, W.; You, W.; Su, Z. M.; Wang, E. B. *J. Am. Chem. Soc.* **2014**, *136*, 5359−5366.
(22) Ibrahim, M.; Haider, A.; Xiang, Y.; Bassil, B. S.; Carey, A. M.; Rullik, L.; Jameson, G. B.; Doungmene, F.; Mbomekallé, I. M.; de Oliveira, P.; Mereacre, V.; Kostakis, G. E.; Powell, A. K.; Kortz, U. *Inorg. Chem.* **2015**, *54*, 6136−6146.
(23) Hervé, G.; Tézé, A. *Inorg. Chem.* **1977**, *16*, 2115−2117.
(24) *SAINT*; Bruker AXS, Inc.: Madison, WI, 2007.
(25) (a) Sheldrick, G. M. *Acta Crystallogr., Sect. A: Found. Crystallogr.* **2008**, *64*, 112−122. (b) Sheldrick, G. M. *SADABS*; University of Göttingen: Göttingen, Germany, 1996.
(26) Sheldrick, G. M. *SHELX-97/2013: Program for Solution of Crystal Structures*; University of Göttingen: Göttingen, Germany, 2013.
(27) Brown, I. D.; Altermatt, D. *Acta Crystallogr., Sect. B: Struct. Sci.* **1985**, *41*, 244−247.
(28) (a) Clemente-Juan, J. M.; Coronado, E.; Galán-Mascarós, J. R.; Gómez-García, C. *Inorg. Chem.* **1999**, *38*, 55−63. (b) Zhao, J. W.; Jia, H. P.; Zhang, J.; Zheng, S. T.; Yang, G. Y. *Chem.—Eur. J.* **2007**, *13*, 10030−10045. (c) Pichon, C.; Dolbecq, A.; Mialane, P.; Marrot, J.; Riviére, E.; Sécheresse, F. *Dalton Trans.* **2008**, *1*, 71−76. (d) Lydon, C.; Sabi, M. M.; Symes, M. D.; Long, D. L.; Murrie, M.; Yoshii, S.; Nojiri, H.; Cronin, L. *Chem. Commun.* **2012**, *48*, 9819−9821. (e) Ibrahim, M.; Xiang, Y.; Bassil, B. S.; Lan, Y.; Powell, A. K.; de Oliveira, P.; Keita, B.; Kortz, U. *Inorg. Chem.* **2013**, *52*, 8399−8408.
(29) Khanra, S.; Kuepper, K.; Weyermüller, T.; Prinz, M.; Raekers, M.; Voget, S.; Postnikov, A. V.; de Groot, F. M. F.; George, S. J.; Coldea, M.; Neumann, M.; Chaudhuri, P. *Inorg. Chem.* **2008**, *47*, 4605−4617.
(30) Prinz, M.; Raekers, M.; Neumann, M.; Kuepper, K.; Khanra, S.; Weyhermüller, T.; Chaudhuri, P. *Z. Phys. Chem.* **2009**, *223*, 145−155.
(31) (a) Liu, J. G.; Ortéga, F.; Sethuraman, P.; Katsoulis, D. E.; Costello, C. E.; Pope, M. T. *J. Chem. Soc., Dalton Trans.* **1992**, 1901−1906. (b) Zhang, X. Y.; Pope, M. T.; Chance, M. R.; Jameson, G. B. *Polyhedron* **1995**, *14*, 1381−1392. (c) Sadakane, M.; Steckhan, E. *Acta Chem. Scand.* **1999**, *53*, 837−841. (d) Sadakane, M.; Steckhan, E. *J. Mol. Catal. A: Chem.* **1996**, *114*, 221−228. (e) Keita, B.; Mialane, P.; Sécheresse, F.; de Oliveira, P.; Nadjo, L. *Electrochem. Commun.* **2007**, *9*, 164−172. (f) Friedl, J.; Al-Oweini, R.; Herpich, M.; Keita, B.; Kortz, U.; Stimming, U. *Electrochim. Acta* **2014**, *141*, 357−366.
(32) (a) Keita, B.; Nadjo, L. Electrochemistry of Isopoly and Heteropoly Oxometalates. In *Encyclopedia of Electrochemistry*; Bard, A. J., Stratmann, M., Eds.; Wiley-VCH: Weinheim, Germany, 2006; Vol. 7, p 607. (b) Lopez, I. X.; Carbo, J. J.; Bo, C.; Poblet, J. M. *Chem. Soc. Rev.* **2012**, *41*, 7537−7571.
(33) (a) Chen, L.; Zhu, K.; Bi, L. H.; Suchopar, A.; Reicke, M.; Mathys, G.; Jaensch, H.; Kortz, U.; Richards, R. M. *Inorg. Chem.* **2007**, *46*, 8457−8459. (b) Chen, L.; Hu, J.; Mal, S. S.; Kortz, U.; Jaensch, H.; Mathys, G.; Richards, R. M. *Chem.—Eur. J.* **2009**, *15*, 7490−7497. (c) Bi, L.-H.; Al-Kadamany, G.; Chubarova, E. V.; Dickman, M. H.; Chen, L.; Gopala, D. S.; Richards, R. M.; Keita, B.; Nadjo, L.; Jaensch, H.; Mathys, G.; Kortz, U. *Inorg. Chem.* **2009**, *48*, 10068−10077.
(34) (a) Hill, C. L.; Brown, R. B. *J. Am. Chem. Soc.* **1986**, *108*, 536−538. (b) Mansuy, D.; Bartoli, J.-F.; Battioni, P.; Lyon, D. K.; Finke, R. G. *J. Am. Chem. Soc.* **1991**, *113*, 7222−7226. (c) Qin, D.; Wang, G.; Wu, Y. *Stud. Surf. Sci. Catal.* **1994**, *82*, 603−608. (d) Guo, J.; Jiao, Q. Z.; Shen, J. P.; Jiang, D. Z.; Yang, G. H.; Min, E. Z. *Catal. Lett.* **1996**, *40*, 43−45. (e) Kholdeeva, O. A.; Donoeva, B. G.; Trubitsina, T. A.; Al-Kadamany, G.; Kortz, U. *Eur. J. Inorg. Chem.* **2009**, *2009*, 5134−5141. (f) Hussain, F.; Bassil, B. S.; Kortz, U.; Kholdeeva, O. A.; Timofeeva, M. N.; de Oliveira, P.; Keita, B.; Nadjo, L. *Chem.—Eur. J.* **2007**, *13*, 4733−4742. (g) Timofeeva, N.; Kholdeeva, O. A.; Jhung, S. H.; Chang, J. S. *Appl. Catal., A* **2008**, *345*, 195−200. (h) Kumar, A.; Srinivas, D.; Ratnasamy, P. *Chem. Commun.* **2009**, 6484−6486. (i) Kholdeeva, O. A.; Derevyankin, A. Yu.; Shmakov, A. N.; Trukhan, E. A. N. N.; Paukshtis, A.; Tuel, V. N.; Romannikov. *J. Mol. Catal. A: Chem.* **2000**, *158*, 417−421.
(35) Kovalenko, I.; Zdyrko, B.; Magasinski, A.; Hertzberg, B.; Milicev, Z.; Burtovyy, R.; Luzinov, I.; Yushin, G. *Science* **2011**, *334*, 75−79.